Communications Engineering

AI-driven System for Non-contact Continuous Nocturnal Blood Pressure Monitoring using Fiber Optic Ballistocardiography

(Supplementary Information)

Contents

Supplementary Note 1—The microbend fiber optic sensing theory

When a sensor mat detects movements caused by breathing or the heartbeat, it applies a change in force (ΔF) or pressure (ΔP) to a bent multimode fiber, altering its deformation amplitude (X) by ΔX. This action changes the transmission coefficient (T) for light travelling along the fiber by ΔT, described as:

$$\Delta T = \left(\frac{\Delta T}{\Delta X}\right) \Delta F \left(k + \frac{AY}{l}\right)^{-1}, \tag{1}$$

where k is the fiber's force constant, A is the cross-sectional area, Y is the Young's modulus, and l is the microbender gap length. Monitoring of breathing rate (BR), breathing waveforms, heart rate (HR), and BCG is done through modulation in optical transmission. For applications requiring highly sensitive pressure sensors, Eq. (1) turns into:

$$\Delta T \approx \frac{\Delta T}{\Delta X} A_p k^{-1} \Delta P, \tag{2}$$

where A_p represents the deformer's area, and ΔP is the pressure change. To maximize the microbend sensitivity, the optical fiber should be constructed to meet a specific spatial frequency (Λ) for the mesh deformer. For step-index multimode fiber, the spatial frequency Λ satisfies the following approximate equation:

$$\Lambda = \sqrt{2}\pi \cdot \frac{a \cdot n_0}{NA}. \tag{3}$$

where a is the fiber core radius, n_0 is the refractive index of the core, and NA is the numerical aperture of the fiber.

The microbending loss occurs as the guided modes are coupled to radiation modes. Effective coupling between the guided modes and radiation modes can be achieved with the spatial frequency Λ given by Eqs. (3) for step-index multimode fibers.

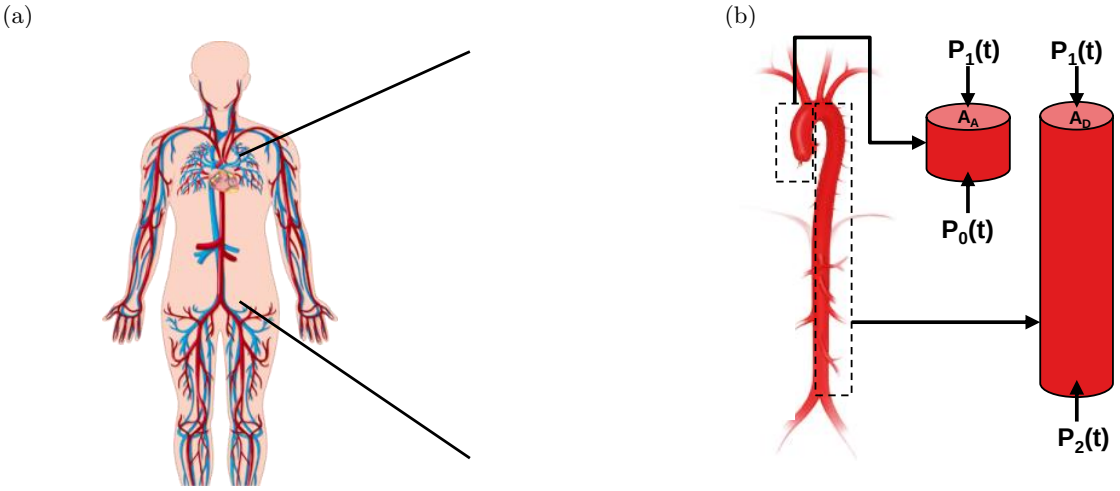

Figure 1: **Modeling the aorta as two tubes in cascade**. (a) Vascular tree of body. (b)The cross-sectional areas of the tubes are denoted by A_A for the ascending aorta and A_D for the descending aorta. The forces exerted on the blood within each tube stem from the blood pressure, $P(t)$, at their respective inlet and outlet points. The notations 0, 1, and 2 represent the inlet of the aorta, the apex of the aortic arch, and the outlet of the aorta, respectively. The BCG waveform is generated by the combination of counter-acting forces from both tubes.

Supplementary Note 2—BCG genesis model and rationale for BP inference

BCG waveform reflects the recoil force of the body when the blood mass is ejected from the heart to the aorta and the direction of the body micro-movement is opposite to the direction of the blood flow. To mathematically analyze the BCG genesis, we can simplify the aorta as two tubes in cascade as shown in Fig. 1. The ascending aorta has an average cross-sectional area of A_{A}, while that of the descending aorta is A_{D}. We denote $P_0(t)$, $P_1(t)$, and $P_2(t)$ as the blood pressure at the inlet of the ascending aorta, the outlet/inlet of the aortic arch, and the outlet of the descending aorta, respectively. By analyzing the equilibrium of recoil forces exerted on the blood mass in the main artery, the BCG waveform in the head-to-foot direction can be mathematically modeled as:

$$F_{\mathrm{BCG}}(t) = A_D[\mathrm{P_1(t)}-\mathrm{P_2(t)}] - A_A[\mathrm{P_0(t)}-\mathrm{P_1(t)}] = A_{\mathrm{D}}[\delta P_{12}(t)] - A_{\mathrm{A}}[\delta P_{01}(t)] \tag{4}$$

Note that $\Delta P_{01}(t) = P_0(t) - P_1(t)$ and $\Delta P_{12}(t) = P_1(t) - P_2(t)$ constitute the BP gradients in the ascending and descending aorta. Therefore, the genesis of the BCG wave is the blood pressure gradient difference between ascending and descending arteries.

The mechanism of the BCG waves revealed by the validated model in equation (4) for the patient example in Fig. 2 is as follows:

- Phase (1): The initial rise of the I wave is propelled by $\delta P_{01}(t)$, as $P_0(t)$ begins to ascend during systole while $P_1(t)$ remains in diastole. The peak of the I wave occurs approximately when $-\delta P_{01}(t)$ is minimal.
- Phase (2): As $P_1(t)$ starts to climb while $P_2(t)$ is still in its diastolic phase, $\delta P_{12}(t)$ increases, eventually neutralizing and surpassing $\delta P_{01}(t)$, leading to the ascent from I to J. The peak of the J wave occurs roughly when $\delta P_{12}(t)$ reaches its maximum.
- Phase (3): With the buildup of $P_2(t)$, $\delta P_{12}(t)$ begins to fall, leading to the descent from J to K. The peak of the K wave is roughly when $P_2(t)$ hits its peak or when $\delta P_{12}(t)$ is at its lowest.
- Phase (4): Following the systolic peak, $P_2(t)$ falls more rapidly than $P_1(t)$, causing an uptick in $\delta P_{12}(t)$. At the same time, $-\delta P_{01}(t)$ sees a temporary increase as $P_0(t)$ rapidly decreases near the dicrotic notch. These events lead to the formation of the L wave.
- Phase (5): Subsequently, $-\delta P_{01}(t)$ returns to zero, while $\delta P_{12}(t)$ slightly dips to a local minimum as the moderate decline in $P_2(t)$. This sequence of events produces the M wave.

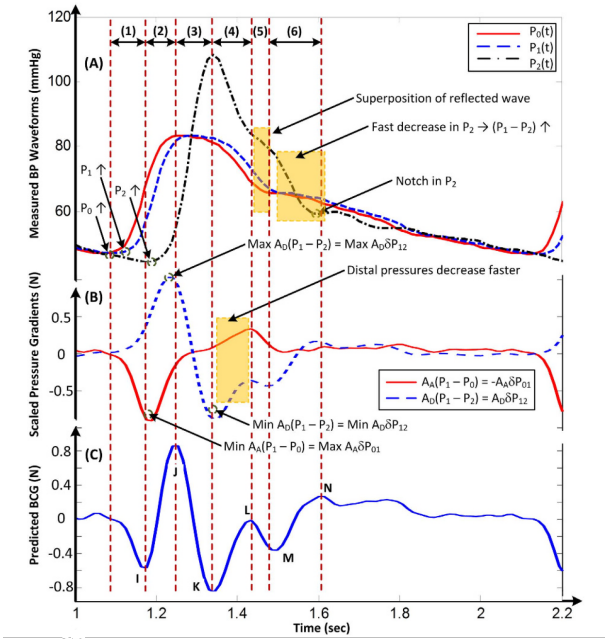

Figure 2: **An example of a BCG waveform predicted via the mathematical model of Eq. 4 [1].** (A) Blood pressure waveforms are recorded at three locations through catheterization in a human subject: the inlet of the aorta (P_0), the apex of the aortic arch (P_1), and the outlet of the aorta (P_2). (B) The BP gradients across the ascending ($A_A \delta P_{01}$) and descending ($A_D \delta P_{12}$) portions of the aorta are calculated using the recorded BP waveforms. The values for cross-sectional areas are common nominal values. (C) The BCG wave was estimated by computing the difference between these BP gradients.

- Phase (6): The rise from M to N is due to the increasing $\delta P_{12}(t)$, driven by the quicker reduction in $P_2(t)$. The peak of the N wave closely matches the time when $\delta P_{12}(t)$ reaches a local maximum, which is triggered by the diastolic notch in $P_2(t)$.

  Therefore, the genesis of BCG signals is interpreted as the blood pressure gradient difference between the ascending and descending aorta. This is the basic rationale that explains why we can use BCG signals as the insightful input for BP inference.

Supplementary Note 3—The inclusion and exclusion criteria

The inclusion and exclusion criteria for the subject recruitment in this study:

Inclusion Criteria:

- Individuals aged between 18-69 years.
- Divide subjects into a healthy group and a hypertension group. The diagnostic criteria for hypertension refer to the "Chinese Guidelines for the Prevention and Treatment of Hypertension 2018".
- Patients who voluntarily signed the informed consent form and agreed to participate in this study.

Exclusion Criteria:

- Individuals with atrial fibrillation or any other arrhythmias that affect peripheral blood flow.
- Patients suffering from shock of any etiology.
- Individuals with Parkinson's disease or other disorders of autonomic movement.
- Cases of Raynaud's syndrome or other conditions affecting blood flow to the extremities.
- Subjects unable to wear blood pressure monitoring devices due to the absence of a middle finger on both hands.
- Individuals who are debilitated, have fractures, deformities due to various causes, or any other condition that prevents the subject from sitting or lying down for extended periods.
- Subjects with dementia, psychiatric illnesses, or other communicative impairments that prevent normal interaction.
- Subjects who refuse to sign the informed consent form and decline participation in this project.

Supplementary Table

Table 1: **Subjects characteristic in different datasets.**

Characteristics	Kansas Dataset	Self-collected Daytime DataSet	Self-collected Nighttime Dataset	ANSI/AAMI/ISO Requirement
Subjects (N)	40	85	33	≥ 85
Age (years)	34 (15)	42.64 (14.33)	48.36 (10.64)	≥ 12
Male (%)	42.5	61.18	48.49	≥ 30
Female (%)	57.5	38.82	51.51	≥ 30
Height (cm)	171 (11)	165.93 (8.73)	163.55 (7.19)	-
Weight (kg)	76 (18)	68.37 (12.83)	67.06 (11.27)	-
BMI (kg/m2)	26 (5.7)	17.54 (4.78)	24.98 (3.34)	-
Hypertension History (%)	2.5	32.94	45.45	-
SBP (mmHg)	120.63 (14.96)	122.01 (18.75)	126.64 (23.15)	-
DBP (mmHg)	67.31 (9.35)	75.50 (11.36)	79.22 (13.61)	-

Table 2: **The definition of 44 fiducial features is based on the delineation of 5 fiducial points.** Different types of fiducial features reflect the 3D structural deformation information of the heart and the transmission states of the blood pressure wave in the aorta.

Feature Type	Feature Name	Description
Extremum	$A(H)$, $A(I)$, $A(J)$, $A(K)$, $A(L)$	The amplitude value of each fiducial point
Displacement	$\|A(H)-A(I)\|$, $\|A(H)-A(J)\|$, $\|A(H)-A(K)\|$, $\|A(H)-A(L)\|$, $\|A(I)-A(J)\|$, $\|A(I)-A(K)\|$, $\|A(I)-A(L)\|$, $\|A(J)-A(K)\|$, $\|A(J)-A(L)\|$, $\|A(K)-A(L)\|$	The amplitude difference between two fiducial point
Time Interval	$T(H,I)$, $T(H,J)$, $T(H,K)$, $T(H,L)$, $T(I,J)$, $T(I,K)$, $T(I,L)$, $T(J,K)$, $T(J,L)$, $T(K,L)$	Time interval between two fiducial point
Time Ratio	$T(H,I)/T$, $T(H,J)/T$, $T(H,K)/T$, $T(I,J)/T$, $T(I,K)/T$, $T(I,L)/T$, $T(J,K)/T$, $T(J,L)/T$, $T(K,L)/T$	Ratios of time inveral to $T = T(H,L)$
Area under the curve	$AUC(H,I)$, $AUC(H,J)$, $AUC(H,K)$, $AUC(H,L)$, $AUC(I,J)$, $AUC(I,K)$, $AUC(I,L)$, $AUC(J,K)$, $AUC(J,L)$, $AUC(K,L)$	Area enclosed by curve $BCG[a,b]$ and line $Y = min(BCG)$.

Table 3: **International standards and protocols for evaluating BP measurements.** Firstly, the mean error (ME) and the standard deviation (SD) were determined to evaluate the performance of the AI system, which is in line with the ANSI/AAMI/ISO standard [2]. This standard mandates that BP devices should have ME and SDE values lower than 5 and 8 mmHg, respectively. Secondly, the mean absolute error (MAE) was calculated to assess the AI system in accordance with the IEEE 1708 standard [3, 4], which categorizes BP devices into four grades regarding different MAE thresholds. Lastly, the cumulative percentage of errors (CPE) within thresholds of 5 (CPE5), 10 (CPE10), and 15 (CPE15) mmHg was computed, which evaluates the system against the criteria set by the British Hypertension Society (BHS) protocol [5]. The BP devices are assigned to four grades according to their CPE at these various levels.

	ANSI/AAMI/ISO	IEEE 1708	BHS		
		MAE	CPE5	CPE10	CPE15
Grade A	-	<5 mmHg	60%	85%	95%
Grade B	-	5-6 mmHg	50%	75%	90%
Grade C	-	6-7 mmHg	40%	65%	85%
Grade D	-	$\geq$ 7 mmHg	Worse than Grade C		
Recommendation for clinical use	ME $\leq$ 5 mmHg SD $\leq$ 8 mmHg	Grades A, B and C	Grades A and B		

Table 4: **Performance of the best-performing personalized model for various bub-populations in the self-collected daytime dataset.** Overall, the results indicate that our system passes the ANSI/AAMI/ISO standard and obtains Grade A under the criteria of IEEE 1708 and BHS.

	SBP						DBP					
	MAE (mmHg)	ME (mmHg)	SD (mmHg)	CPE5 (%)	CPE10 (%)	CPE15 (%)	MAE (mmHg)	ME (mmHg)	SD (mmHg)	CPE5 (%)	CPE10 (%)	CPE15 (%)
All-subject	4.78	0.13	7.02	66.07	88.00	95.25	2.41	0.08	3.50	87.83	97.86	99.62
Different BP levels												
Normotensive	4.33	0.23	6.38	69.67	90.51	96.39	2.24	0.12	3.31	89.83	98.11	99.64
Stage-1 HBP	5.96	-0.71	7.97	52.47	80.25	94.09	2.99	-0.36	3.99	80.32	97.81	99.69
Stage-2 HBP	9.36	2.50	11.39	30.97	61.93	78.70	4.77	0.99	5.97	61.51	89.56	98.45
Different age levels												
(18, 35]	2.89	-0.17	4.32	84.41	96.68	98.87	1.48	-0.08	2.18	96.61	99.43	99.90
(35, 55]	5.89	0.61	8.40	56.57	82.78	92.70	2.97	0.29	4.13	82.10	96.57	99.47
(55, 65]	5.47	-0.23	7.55	57.28	85.86	95.06	2.76	-0.10	3.80	85.45	97.97	99.46

Stage-1 HBP and Stage-2 HBP indicate stage-1 hypertension and stage-2 hypertension, respectively.

Table 5: **Performance of the best-performing personalized model for various sub-populations in the self-collected nocturnal dataset.** Overall, the results indicate that our system passes the ANSI/AAMI/ISO standard for DBP inference, but fails for SBP inference. The system performance reaches Grade C under the criteria of IEEE 1708 and Grade B under the criteria of BHS. Error bars represent the range of data within 1.5 times the interquartile range (IQR) from the first quartile (Q1) to the third quartile (Q3).

	SBP						DBP					
	MAE (mmHg)	ME (mmHg)	SD (mmHg)	CPE5 (%)	CPE10 (%)	CPE15 (%)	MAE (mmHg)	ME (mmHg)	SD (mmHg)	CPE5 (%)	CPE10 (%)	CPE15 (%)
All-subject	6.91	-0.26	9.43	48.84	76.64	89.58	3.46	-0.15	4.75	76.58	95.31	99.02
Different BP levels												
Normotensive	7.11	-0.31	7.58	46.63	75.12	89.38	3.56	-0.19	4.80	75.09	95.11	99.09
Stage-1 HBP	7.37	-0.43	10.56	51.09	76.15	86.55	3.72	-0.19	5.37	76.06	91.89	97.77
Stage-2 HBP	11.27	1.70	13.05	21.36	44.60	70.45	5.66	0.82	6.59	44.05	90.67	99.18
Different age levels												
(18, 35]	4.59	-0.04	6.55	65.70	86.60	96.19	2.29	-0.05	3.28	86.59	99.04	99.91
(35, 55]	7.13	0.04	9.79	48.20	76.87	88.83	3.59	0.01	4.99	76.88	94.13	98.63
(55, 65]	7.69	-1.38	9.59	39.82	69.51	87.65	3.86	-0.74	4.79	69.11	96.56	99.76

Stage-1 HBP and Stage-2 HBP indicate stage-1 hypertension and stage-2 hypertension, respectively.

Supplementary Figure

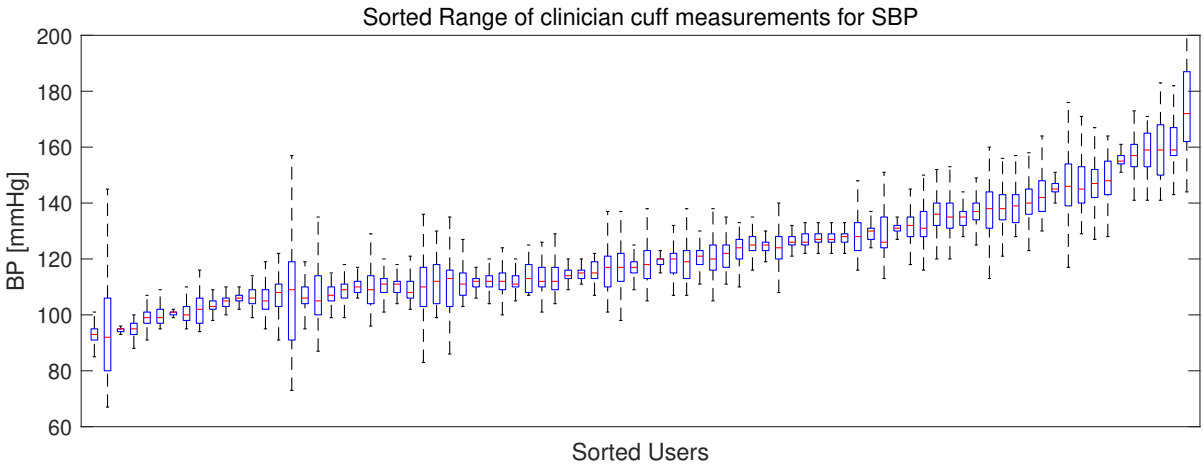

Figure 3: **SBP dynamics of daytime dataset**. Blood pressure range as measured by the trained observer (Caretaker measurement) for each subject (in a column). Subjects are organized by increasing systolic baseline pressure. Overall, the systolic pressure ranges from 67 to 200+ mmHg. Individually, the average systolic pressure dynamics (max-min) is 36.1 $\pm$ 19.5 mmHg. Error bars represent the range of data within 1.5 times the interquartile range (IQR) from the first quartile (Q1) to the third quartile (Q3).

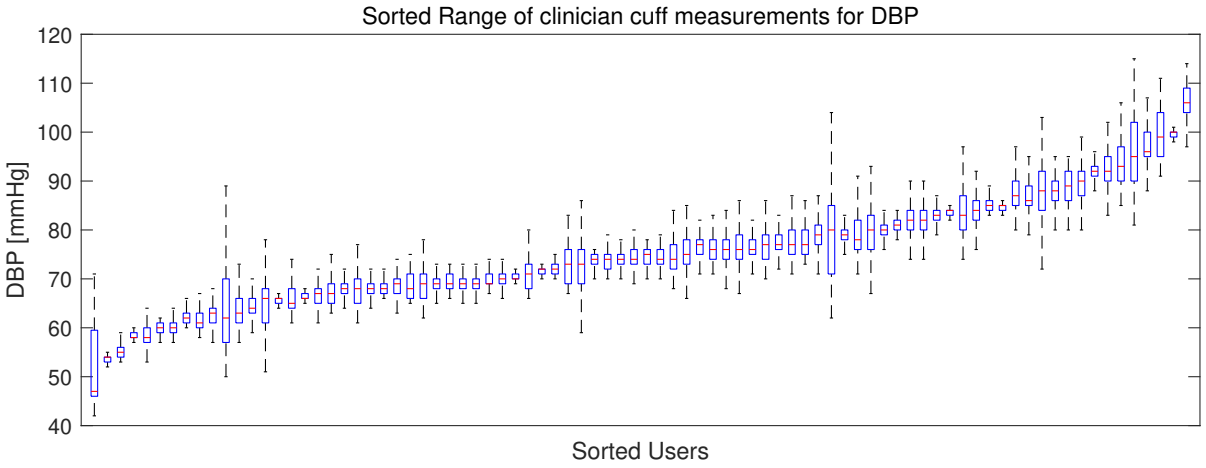

Figure 4: **DBP dynamics of daytime dataset**.Blood pressure range as measured by the trained observer (Caretaker measurement) for each subject (in a column). Subjects are organized by increasing diastolic baseline pressure. Overall, the diastolic pressure ranges from 42 to 115 mmHg. Individually, the average diastolic pressure dynamics (max-min) is 18.4 $\pm$ 9.7 mmHg. Error bars represent the range of data within 1.5 times the interquartile range (IQR) from the first quartile (Q1) to the third quartile (Q3).

Figure 5: **SBP dynamics of nocturnal dataset**. Blood pressure range as measured by the trained observer (Caretaker measurement) for each subject (in a column). Subjects are organized by increasing systolic baseline pressure. Overall, the systolic pressure ranges from 55 to 200+ mmHg. Individually, the average systolic pressure dynamics (max-min) is 55.3 $\pm$ 39.4 mmHg. Error bars represent the range of data within 1.5 times the interquartile range (IQR) from the first quartile (Q1) to the third quartile (Q3).

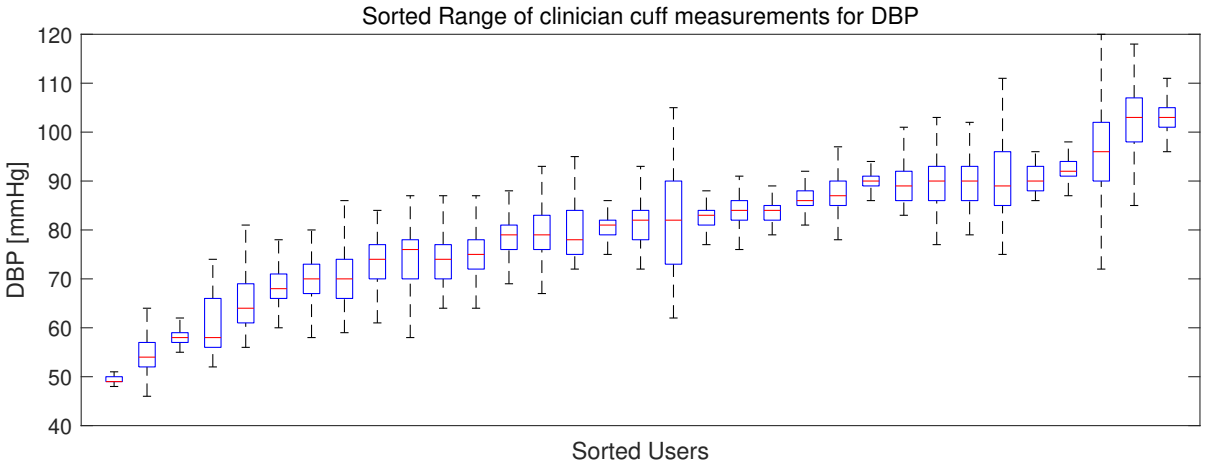

Figure 6: **DBP dynamics of nocturnal dataset**.Blood pressure range as measured by the trained observer (Caretaker measurement) for each subject (in a column). Subjects are organized by increasing diastolic baseline pressure. Overall, the diastolic pressure ranges from 46 to 118 mmHg. Individually, the average diastolic pressure dynamics (max-min) is 27.7 $\pm$ 19.7 mmHg. Error bars represent the range of data within 1.5 times the interquartile range (IQR) from the first quartile (Q1) to the third quartile (Q3).

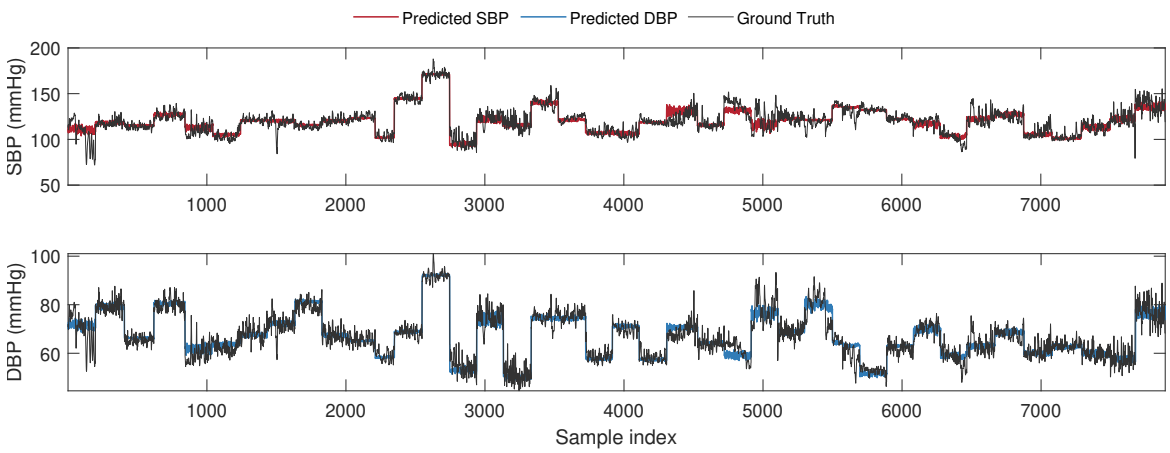

Figure 7: **Time series plots for all subjects in the open-source dataset.**

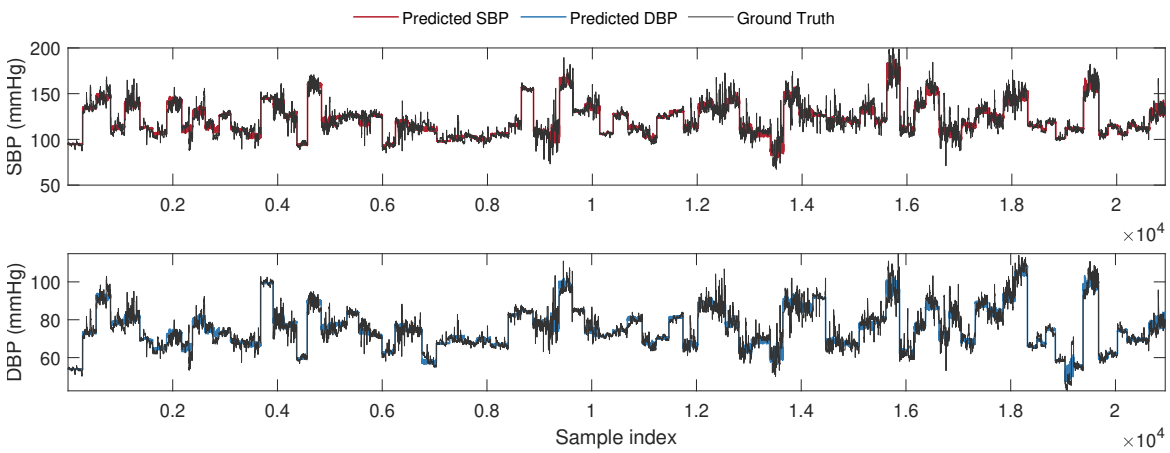

Figure 8: **Time series plots for all subjects in the self-collected daytime dataset.**

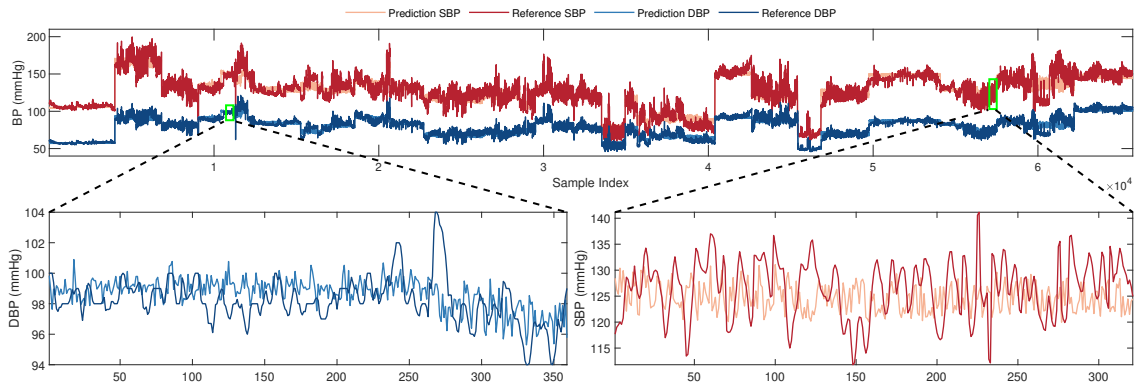

Figure 9: **Time series plots for all subjects in the self-collected nocturnal dataset.**

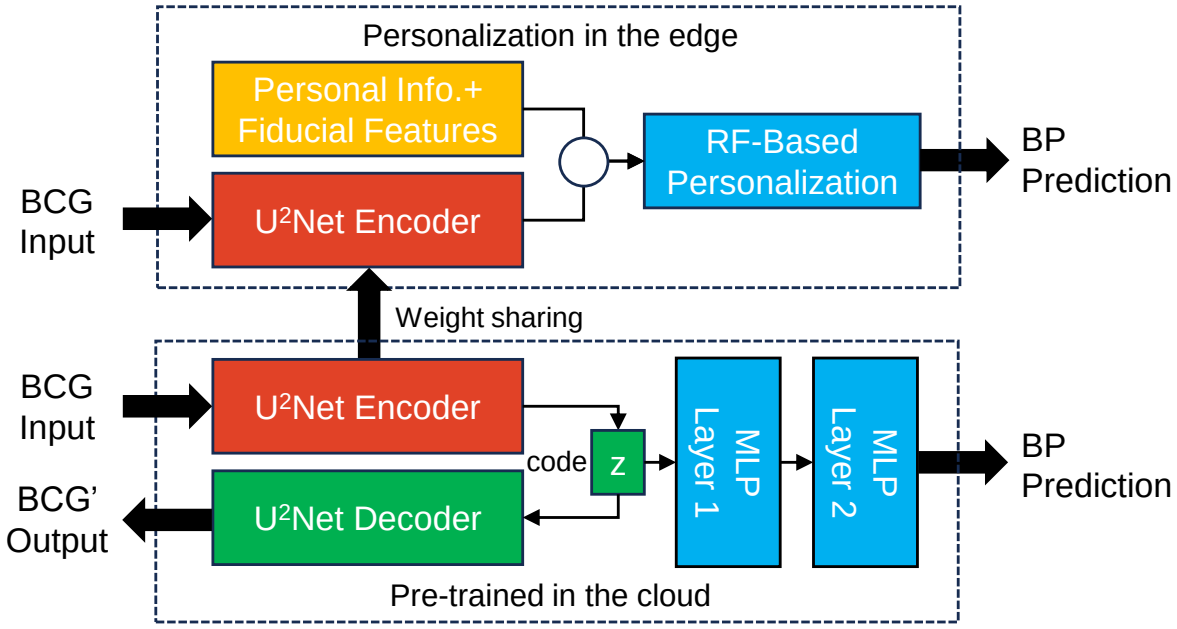

Figure 10: **Block diagrams of pre-training and personalization of AI model.**

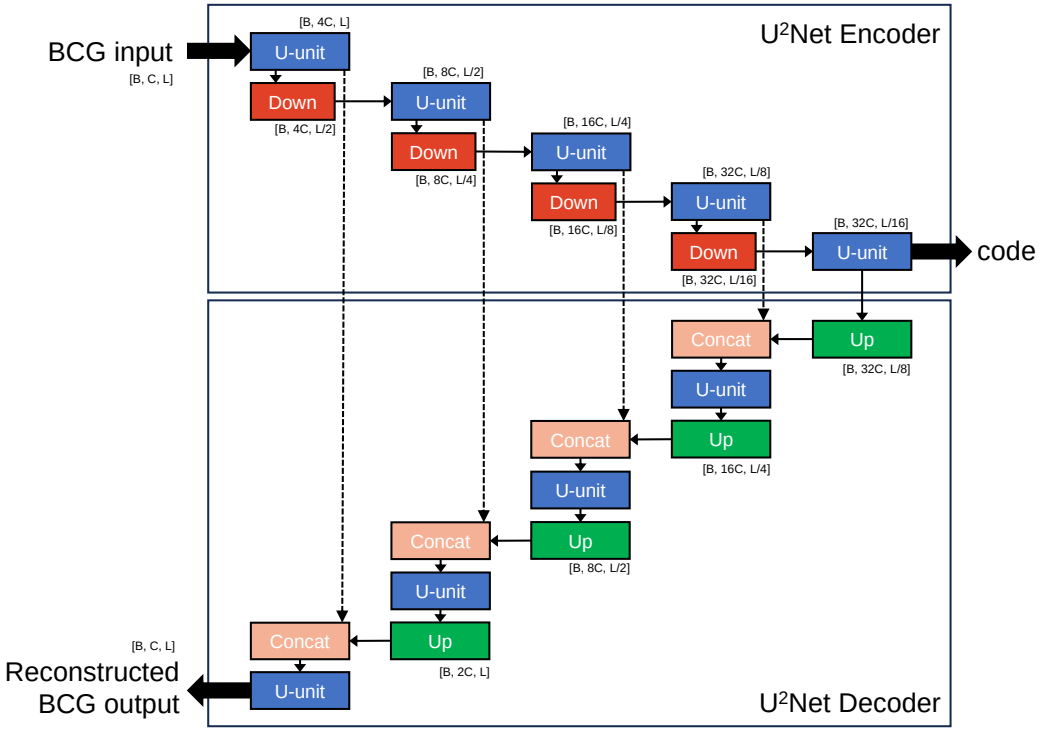

Figure 11: **The U^2-net structure**. The U^2-net is composed of multiple nested U-units.

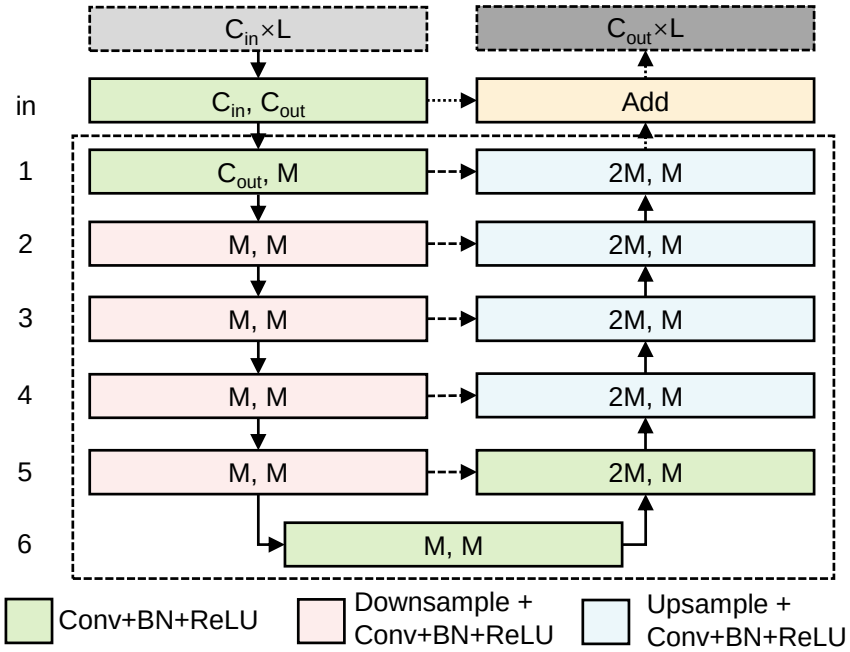

Figure 12: **The detailed architecture for U-unit.** It is a U-shape encoder-decoder with a residual connection.

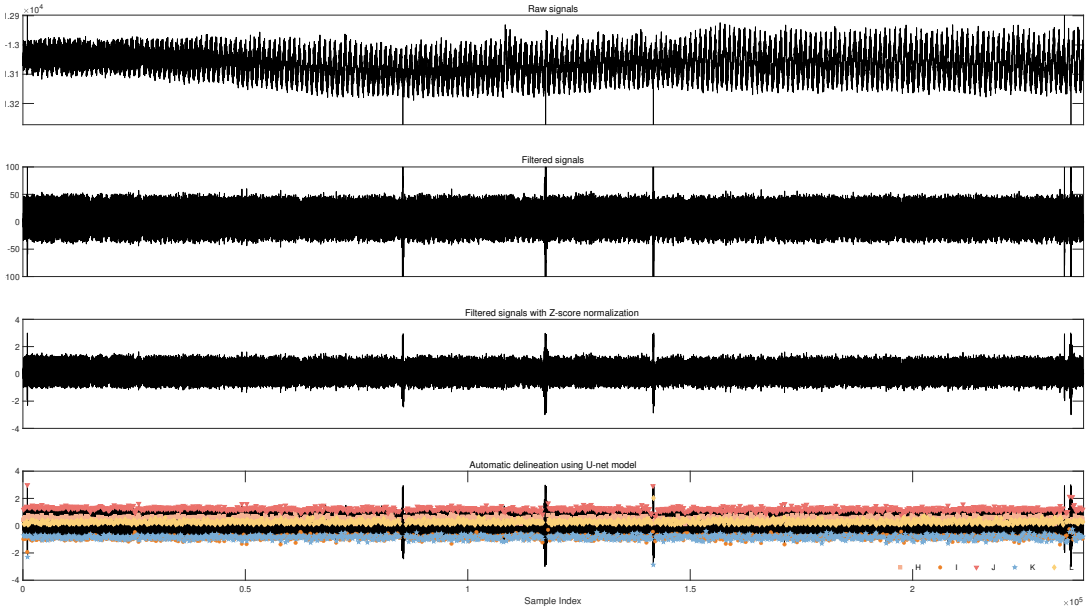

Figure 13: **A typical session of BCG signals during sleep from subject N001.** The subject is stationary during sleep and the raw signals collected from the optical fiber sensor are slightly affected by the respiration motion. However, the respiration motion artifact is easily removed after signal processing.

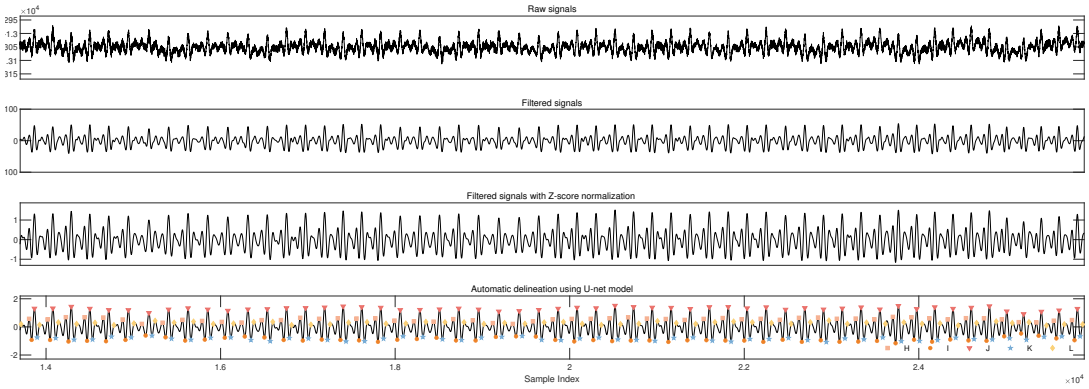

Figure 14: **A zoom-in figure from Fig. 13.** The last row shows accurate automatic delineation of fiducial points (H, I, J, K, L).

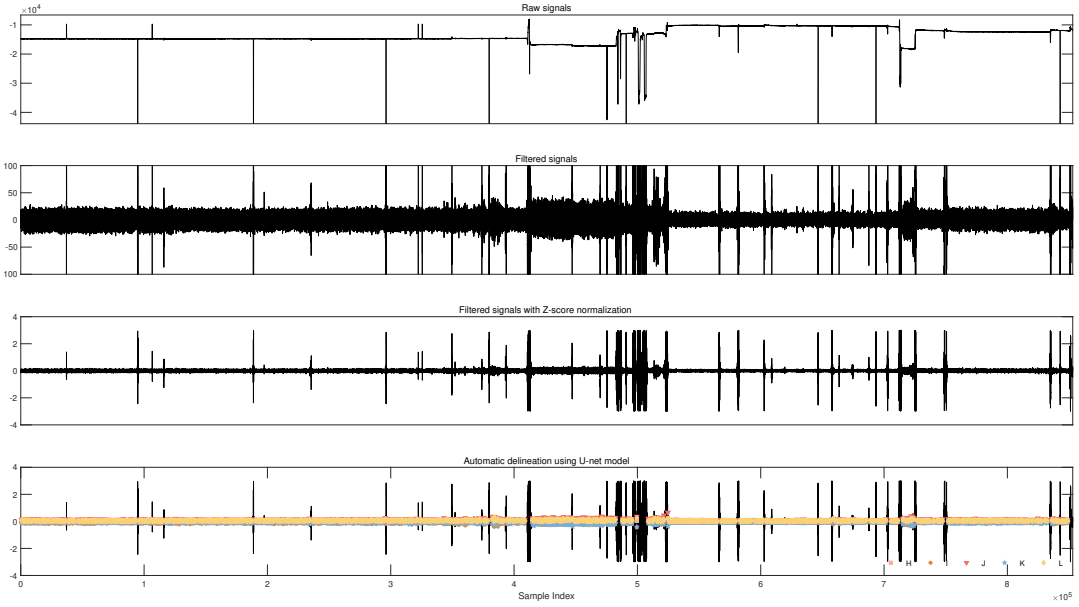

Figure 15: **A noisy session of BCG signals during sleep from subject N002.** When the user sleeps at night, there may be some body movements that cause a large impact on the sensor mat. This figure shows a relatively noisy session where discontinuous jumps can be observed in the middle part of the raw signals row due to body movements. The zoom-in details can be seen in Fig. 16 and Fig. 17

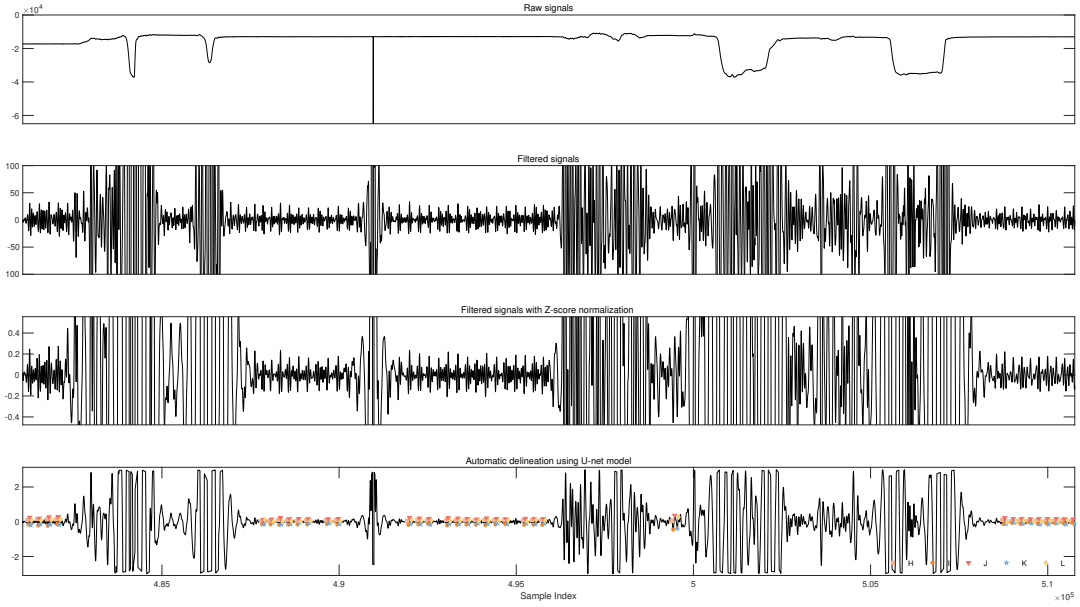

Figure 16: **A zoom-in figure from Fig. 15.** The motion artifacts caused by body movement have a much higher order of magnitude than that of heartbeat signals (BCG). It is easy to detect the noisy segment after normalization using the threshold-based outlier detection method. In addition, our U-net automatic delineation is trained with standard BCG cycles and it has the ability to identify the noisy segment as well.

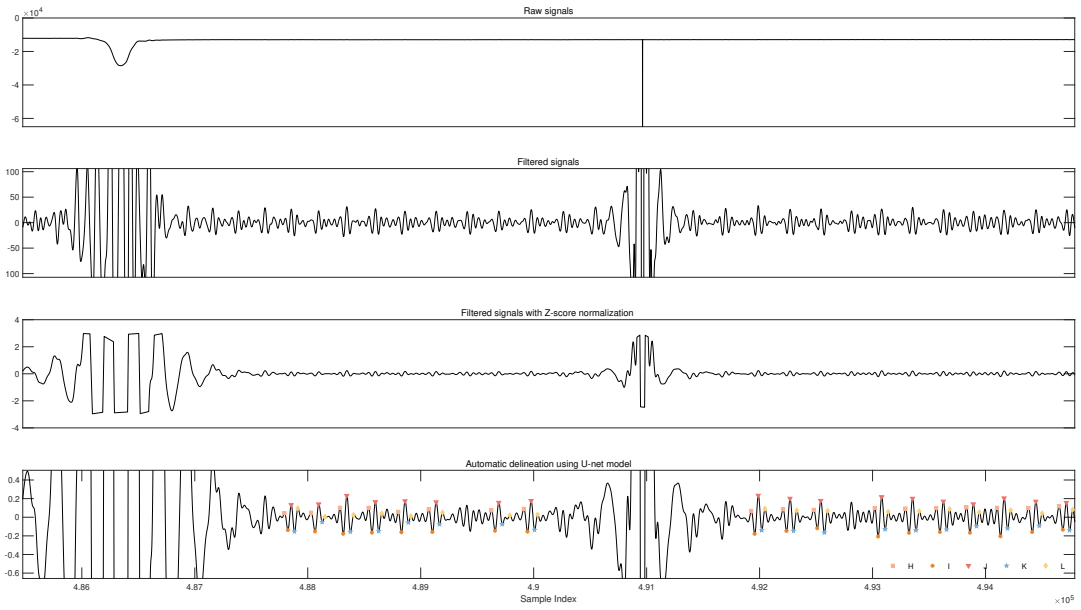

Figure 17: **A further zoom-in figure from Fig. 16.** After Z-score normalization, the detection outlier sample points will be replaced using the results from linear interpolation. Consequently, in the third row, the noisy signals exhibit several cut-off parts, further enhancing their discriminability compared to normal BCG signals. The U-net automatic delineation will not label fiducial points on these noisy segments, thus excluding them from model input.

Supplementary References

[1] Chang-Sei Kim, Stephanie L Ober, M Sean McMurtry, Barry A Finegan, Omer T Inan, Ramakrishna Mukkamala, and Jin-Oh Hahn. Ballistocardiogram: Mechanism and potential for unobtrusive cardiovascular health monitoring. *Scientific reports*, 6(1):31297, 2016.

[2] George S Stergiou, Bruce Alpert, Stephan Mieke, Roland Asmar, Neil Atkins, Siegfried Eckert, Gerhard Frick, Bruce Friedman, Thomas Graßl, Tsutomu Ichikawa, et al. A universal standard for the validation of blood pressure measuring devices: Association for the advancement of medical instrumentation/european society of hypertension/international organization for standardization (aami/esh/iso) collaboration statement. *Hypertension*, 71(3):368–374, 2018.

[3] Ieee standard for wearable cuffless blood pressure measuring devices. *IEEE Std 1708-2014*, pages 1–38, 2014.

[4] Ieee standard for wearable, cuffless blood pressure measuring devices - amendment 1. *IEEE Std 1708a-2019 (Amendment to IEEE Std 1708-2014)*, pages 1–35, 2019.

[5] Eoin O'Brien, James Petrie, William Littler, Michael De Swiet, Paul L Padfield, Douglas Altman, Martin Bland, Andrew Coats, Neil Atkins, et al. The british hypertension society protocol for the evaluation of blood pressure measuring devices. *J hypertens*, 11(Suppl 2):S43–S62, 1993.